Density functional theory investigation of the coordination of Zn(II)-tetraphenylporphyrin with 1,2,3-triazole ligands

Jean-François Nierengarten

Journal of Porphyrins and Phthalocyanines
J. Porphyrins Phthalocyanines 2023; **27**: 1253–1262
DOI: 10.1142/S1088424623500803

Published at https://www.worldscinet.com/jpp/

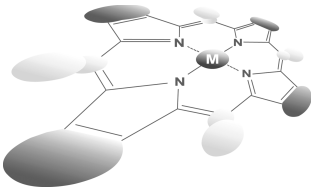

Density functional theory investigation of the coordination of Zn(II)-tetraphenylporphyrin with 1,2,3-triazole ligands

Jean-François Nierengarten*

Laboratoire de Chimie des Matériaux Moléculaires, Université de Strasbourg et CNRS (UMR 7042, LIMA), Ecole Européenne de Chimie, Polymères et Matériaux (ECPM), 25 rue Becquerel, 67087 Strasbourg Cedex 2, France

Received 4 February 2023
Accepted 16 March 2023

Dedicated to Prof. Jonathan L. Sessler on the occasion of his 65th birthday

ABSTRACT: In this paper, we report density functional theory (DFT) studies to fully understand the coordination interactions between 1,4-disubstituted 1,2,3-triazole derivatives and the metal center of Zn(II)-porphyrins. Coordination through the most electron-rich N3 atom of the triazole heterocycle is more favorable. However, the energy difference between the N2- and N3-coordinated isomers is moderate and the less stable is likely also present in the solution. The binding of 1,4-disubstituted 1,2,3-triazole ligands to oxidized and reduced Zn(II)-porphyrins has been also investigated. Upon reduction, the binding interactions are extremely weak and the formation of the complex is not favorable anymore. In contrast, the binding energy is considerably increased upon oxidation of the Zn(II)-porphyrin moiety thus leading to more stable complexes. The calculations fully support experimental findings and explain the differences observed for the redox potentials of complexed and uncomplexed Zn(II)-porphyrin residues.

KEYWORDS: density functional theory, metalloporphyrin, *N*-ligand, apical coordination, electrochemistry.

INTRODUCTION

The copper(I)-catalyzed alkyne-azide cycloaddition (CuAAC) is without any doubt the most emblematic reaction in the field of click chemistry [1–2]. Owing to its reliability, specificity, and efficiency, the CuAAC reaction has become an extremely useful synthetic tool. It has been used to prepare a rich variety of compounds for applications in all fields of science [2]. As a result, 1,2,3-triazole rings are more and more often present in the molecular systems produced over the past two decades. For this reason, the chemical and physical properties of 1,2,3-triazole derivatives have been also intensively investigated [3]. In particular, it has been shown that 1,2,3-triazoles are potential ligands for transition metals due to the presence of two unsubstituted sp^2-hybridized N atoms in their heterocyclic structure [4]. In a monodentate coordination mode, 1,4-disubstituted-1,2,3-triazoles are typically coordinated through the N3 nitrogen which is the most electron-rich [4]. Such ligands are also interacting with metalloporphyrins but the interaction is rather weak when compared to pyridine or imidazole ligands [5]. This has been ascribed to the significantly lower basicity of the 1,2,3-triazole ring. The triazole-metalloporphyrin interaction alone is therefore not particularly attractive for the preparation of stable supramolecular ensembles. Nonetheless, it has been successfully used by Osuka and co-workers for the construction of well-defined macrocyclic supramolecular assemblies from triazole-appended Zn(II)-porphyrin derivatives [6–7]. They have for example shown that Zn(II)-porphyrin **1** can form a cofacial dimer by mutual coordination of the triazole substituents of one porphyrin to the Zn(II) center of the other one (Fig. 1). In this case, multiple interactions and cooperative effects ensure the stability of the macrocyclic ensemble. The X-ray crystal structure of the supramolecular dimer revealed coordination through the

*Correspondence to: Jean-François Nierengarten, e-mail: nierengarten@unistra.fr

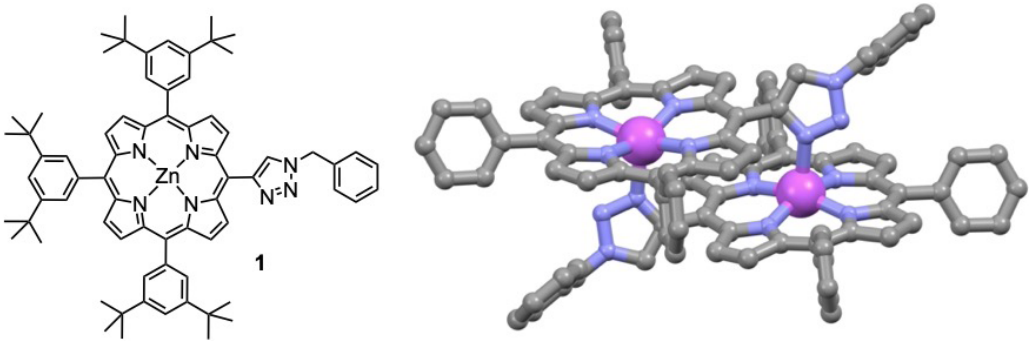

Fig. 1. Zn(II)-porphyrin **1** and X-ray crystal structure of the cofacial dimer (the *t*Bu substituents have been omitted for clarity) [6].

N3 nitrogen of the triazole ring [6]. Coordination of the N2 nitrogen would not allow for the concerted formation of a dimer in this particular case and to the best of our knowledge, the preferential intermolecular coordination of metalloporphyrins with triazole ligands through the N3 nitrogen in solution has not been demonstrated so far.

On the other hand, intramolecular triazole-metalloporphyrin interactions have been also observed in several systems [8–13]. This is for example the case of [2] rotaxanes in which a triazole group of the axle is coordinating the metal center of a metalloporphyrin-containing macrocyclic component [8–10]. Beer and co-workers have shown that this intramolecular coordination preorganizes the rotaxane binding cavity and thus dramatically enhances its anion binding affinities [8]. In other examples, the intramolecular coordination interactions have been used to control the position of the metalloporphyrinic macrocycle onto the molecular axle of the rotaxane [9] or to modulate the excited state deactivation of porphyrin-fullerene conjugates [10]. As part of this research, our group has shown that intramolecular triazole-Zn(II)porphyrin interactions can be used to control the conformation of multiporphyrinic arrays **2** and **3** constructed on a pillar[5]arene scaffold (Fig. 2) [12].

For both **2** and **3**, intramolecular coordination interactions between some 1,2,3-triazole linkers and metal centers of neighboring Zn(II)-porphyrin moieties are responsible for their partial folding at room temperature. At high temperatures, the weak intramolecular coordination interactions are disrupted and both **2** and **3** adopt a fully open structure. In contrast, lowering the temperature favors the association thus leading to the folding of **2** and **3**.

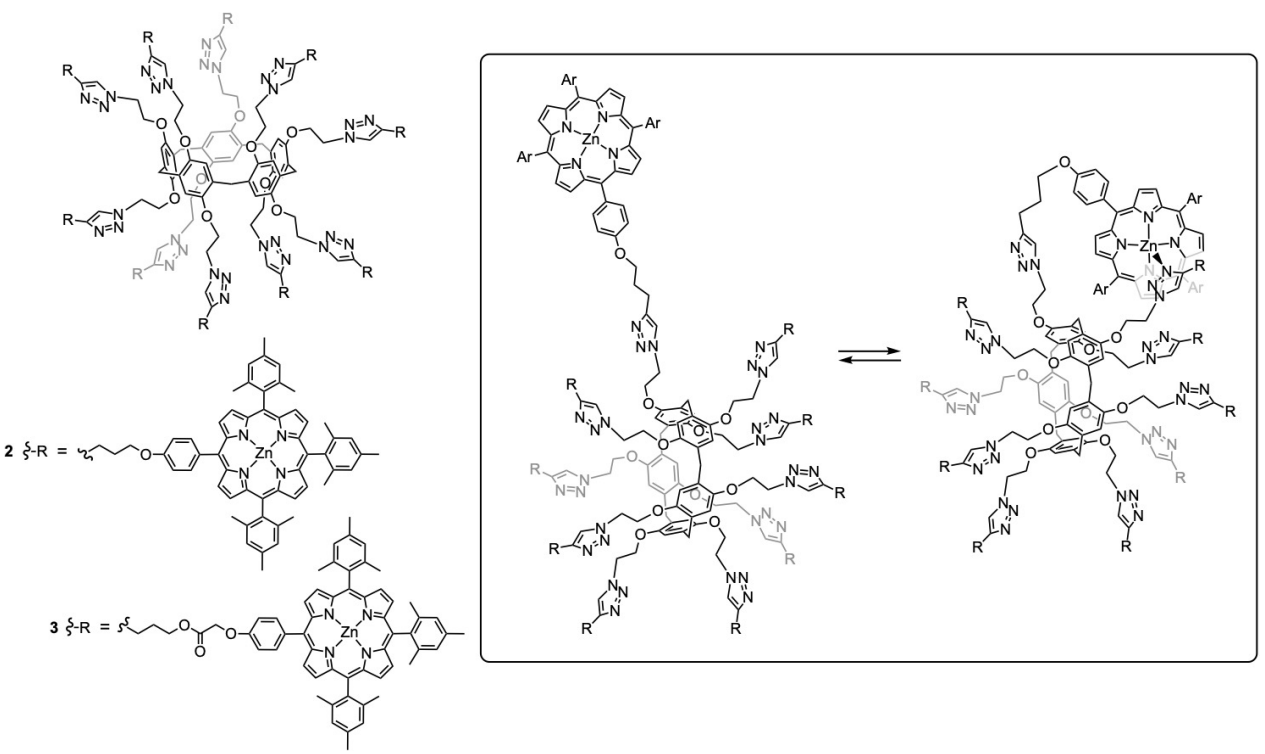

Fig. 2. Multi-Zn(II)-porphyrin arrays **2** and **3**. The inset shows a schematic representation of the dynamic conformational equilibrium resulting from the intramolecular coordination of a 1,2,3-triazole moiety to a neighboring Zn(II)-porphyrin subunit in **2**.

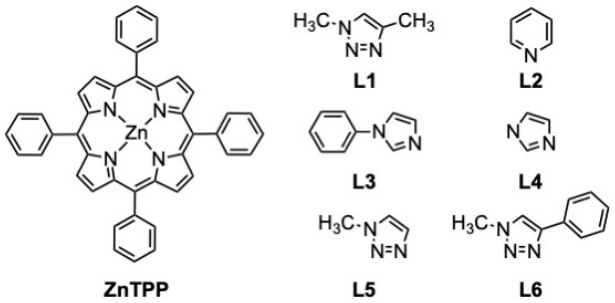

Chart 1. Structure of the compounds used for the theoretical investigations.

Moreover, we have also shown that the degree of folding can be fully controlled by an electrochemical input. Upon reduction of their ten peripheral Zn(II)-porphyrin subunits, total decoordination occurs thus leading to fully unfolded decaanions. In contrast, oxidation of the peripheral porphyrins generates folded decacations in which all the metal centers of the peripheral Zn(II)porphyrin radical cations are coordinated with a triazole unit. In this paper, we now report density functional theory (DFT) studies to fully understand the coordination interactions between 1,4-disubstituted 1,2,3-triazole derivatives and the metal center of Zn(II)-porphyrins. For this purpose, 1,4-dimethyl-1,2,3-triazole (**L1**) and Zinc(II) 5,10,15,20-(tetraphenyl)porphyrin (**ZnTPP**) have been selected for the theoretical calculations (Chart 1). For comparison purposes, calculations have been also performed with pyridine (**L2**) and 1-phenylimidazole (**L3**) as their coordination with metalloporphyrin is well documented and understood [14]. Additionally, reference ligands **L4-6** have been also computed.

EXPERIMENTAL

All DFT calculations were performed with Spartan 20 [15–16] on a Mac Pro with 8 cores and 3 GHz Intel Xeon E5 processors. For the pK_A calculations of the ligands, geometry optimization as well as subsequent frequency analysis at 298.15 K were performed at the B3LYP/6-311+G(2df,2p) level using the CPCM model [17] with the dielectric constant of water (78.30). As revealed by the frequency analysis, imaginary frequencies were absent in all ground states. For ligands **L1-6**, the following equilibrium was considered to calculate the $pK_a(LH^+)$ values:

$$(LH^+)_{aq} \rightarrow (L)_{aq} + (H^+)_{aq} \quad (1)$$

The pK_a of LH^+ was calculated from

$$\Delta G_{aq} = G(L)_{aq} + G(H^+)_{aq} - G(LH^+)_{aq} \quad (2)$$

$$pK_a(LH^+) = \Delta G_{aq}/2.303RT \quad (3)$$

where R is the gas constant, T is the temperature, and ΔG_{aq} is the free energy of the reaction. For the calculations, the Gibbs free energy of the solvated proton ($G(H^+)_{aq}$ = -1130.85 kJ/mol) reported by Coe and co-workers has been used [18]. An error of at least 8 kJ/mol is usually assumed to correspond to *ca*. 1.5 pK_a units. To avoid the uncertainties related to the proton-free energy, the pK_a values were also computed by using isodesmic reactions and the experimental pK_a data of a reference system (pyridine, pK_a (pyridine)$_{exp}$ = 5.23):

$$(LH^+)_{aq} + (\text{pyridine})_{aq} \rightarrow (L)_{aq} + (\text{pyridineH}^+)_{aq} \quad (4)$$

$$\Delta G_{exchange} = G(L)_{aq} + G(\text{pyridineH}^+)_{aq} - G(LH^+)_{aq} - G(\text{pyridine})_{aq} \quad (5)$$

$$pK_a(LH^+) = (\Delta G_{exchange}/2.303RT) + pK_a(\text{pyridine})_{exp} \quad (6)$$

For the coordination of **ZnTPP** with the various *N*-ligands, geometry optimization of all the compounds was first performed in the gas phase with the B3LYP functional using the 6-31G(d) basis set. The structures were further optimized at the same level using the CPCM model in solvents of different polarities, namely CH_2Cl_2 (dielectric constant of 8.82) and DMF (dielectric constant of 37.22). In all the cases, the frequencies were computed at the same level to confirm that each optimized structure is an energy minimum and to evaluate its zero-point vibration energy (ZPVE) and thermal corrections at 298.15 K. The UV/vis spectra of **ZnTPP** and **ZnTPP-L1-3** were also calculated in the gas phase at the TD-B3LYP/6-31G(d) level of theory. Single-point energy calculations were performed at the B3LYP/6-311+G** level to evaluate the distortion and interaction energies. For this purpose, the electronic energies of the **ZnTPP** and **L1-3** fragments from the **ZnTPP-L1-3** structures were also computed.

The Boltzmann distribution was calculated from:

$$N_i/N = \exp(-E_i/kT)/\sum_j \exp(-E_j/kT) \quad (7)$$

where N_i is the number of molecules in conformation i, N is the total number of molecules in the system, E_i is the energy of state i, T is the equilibrium temperature of the system, and k is the Boltzmann constant.

The coordinates of all the B3LYP/6-31G(d) optimized structures are reported in the electronic supplementary information together with the corresponding DFT computed energies, the pK_a calculations, the distortion/interaction analysis, and the frontier molecular orbitals (FMO).

RESULTS AND DISCUSSION

As a preliminary step, the pK_a values of ligands **L1-3** were calculated in an aqueous solution. For this purpose, the neutral and the protonated form of **L1-3** were calculated in water using the CPCM (conductor-like polarizable continuum model) approach [17]. CPCM does not account for explicit solvent-solute interactions

such as H-bonds or hydrophobic effects. However, such simple continuum calculations typically provide good qualitative trends for the investigated systems [19–20]. To further evaluate the calculated pK_a values, calculations were also performed on related systems for which experimental pK_a values are available, namely imidazole (**L4**), 1-methyl-1,2,3-triazole (**L5**), and 1-methyl-4-phenyl-1,2,3-triazole (**L6**). Whereas only one protonable *N* atom is present in pyridines and imidazoles, the situation is more complex for 1-substituted 1,2,3-triazoles. Effectively, the 1,2,3-triazole ring contains two basic sp^2-hybridized *N* atoms, namely N2 and N3, and two protonated forms are possible (Fig. 3). Close inspection of the atomic charge in the calculated triazole derivatives revealed more negative values for N3 when compared to N2 in all the cases. Protonation should be favored on the more electron-rich *N* atom and, effectively, in all the cases, the triazoliums protonated in the N3 positions were found more stable than the corresponding cations protonated in the N2 position (Fig. 3). This is in perfect agreement with related experimental and theoretical results reported in the literature [20a]. The difference in free energy between the two triazolium isomers of **L1**, **L5,** and **L6** is rather large (32.5 to 36.9 kJ/mol, see Fig. 3), thus the Boltzman population of the less stable cation at 298.15 K is negligible (0.00020 to 0.00012%). Therefore, for the pK_a calculation of the triazolium derivatives, only the most stable protonated forms were considered. As anticipated, the triazole ligands are all significantly less basic when compared to pyridines and imidazoles. Overall, direct calculations of the pK_a values with Eq. (3) at the B3LYP/6-311+G(2df,2p) level in water gave a correct trend but comparison with the experimental values reveals errors up to almost 2 pK_a units. In contrast, the difference between the calculated and the experimental pK_a values are less important by using isodesmic reactions with pyridine as a reference system. The relative basicity of **L1-6** can also be simply evaluated by the difference in the natural atomic charge

Table 1. Experimental and calculated $pK_a(LH^+)$ values of 1,4-dimethyl-1,2,3-triazole (**L1**), pyridine (**L2**), 1-phenylimidazole (**L3**) imidazole (**L4**), 1-methyl-1,2,3-triazole (**L5**) and 1-methyl-4-phenyl-1,2,3-triazole (**L6**). The Gibbs free energy values calculated at the B3LYP/6-311+G(2df,2p) level in water have been used for the $pK_a(LH^+)$ calculations.

Compound	$pK_a(LH^+)$ Calculated from Eq. (3)	$pK_a(LH^+)$ Calculated from Eq. (6) with **L2** as reference	$pK_a(LH^+)$ Experimental value
L1	1.14	2.05	
L2	4.32		5.23[a]
L3	5.02	5.93	
L4	5.97	6.88	6.95[a]
L5	-0.61	0.30	1.25[a]
L6	-0.86	0.05	0.05[a]

[a]From ref. [20].

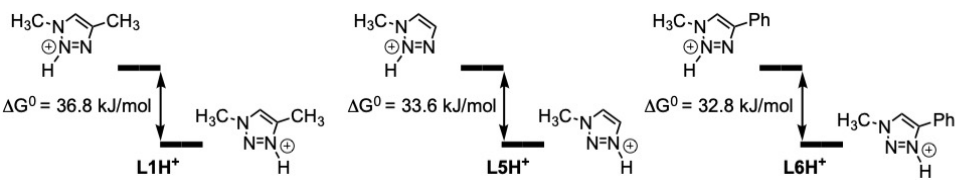

(a)

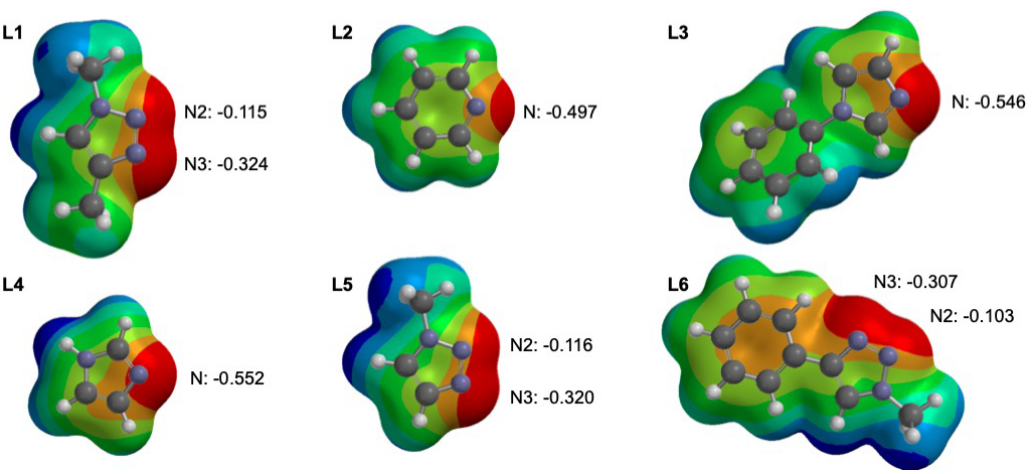

(b)

Fig. 3. (a) Relative Gibbs free energy at 298.15 K (ΔG^0) calculated at the B3LYP/6-311+G(2df,2p) level for the isomeric protonated forms of **L1**, **L5,** and **L6**. (b) Electrostatic potential map of **L1-6** and natural atomic charge of their unsubstituted sp^2-hybridized N atoms.

of the *N* atom involved in the protonation. Increased basicity is systematically associated with an increased natural atomic charge of the *N* atom. This first series of calculations revealed that triazoles are only poorly basic and as such, they should be only weak ligands for **ZnTPP**. This has been already experimentally confirmed by the difference in the binding constant (K_a) values obtained for the association of 1*H*-1,2,3-triazole (480 M^{-1}) and pyridine (5800 M^{-1}) with **ZnTPP** in toluene at room temperature [5].

The geometries of the **ZnTPP-L1-3** complexes, **ZnTPP** and **L1-3** were optimized at the B3LYP/6-31G(d) level in both the gas phase and in solvents of different polarities (CH_2Cl_2 and DMF) using the CPCM model. The B3LYP functional combined with 6-31G* or higher basis set has proven its ability to display and predict the physicochemical properties of porphyrin derivatives and large metalloporphyrin supramolecular ensembles [21–23]. Relevant thermodynamic and structural parameters of the optimized **ZnTPP-L1-3** complexes are summarized in Table. 2.

In the particular case of **ZnTPP-L1**, the two possible isomers resulting from the coordination of the metal center through N2 or N3 of the 1,2,3-triazole ligand have been calculated. As shown in Fig. 4, the coordination of **L1** with the more electronegative *N* atom is favored. However, the free energy difference between the N2- and N3-coordinated isomers is less important when compared to the one calculated for the two isomeric protonated forms of **L1**. In the case of **ZnTPP-L1**, the Boltzmann population of the less stable N2-coordinated isomer is not negligible anymore. In the gas phase, the N3/N2 isomer distribution was found to be 96/4. In CH_2Cl_2 and DMF, the difference in Gibbs free energy was slightly increased when compared to the gas phase. Accordingly, the Boltzmann population of the N2 isomer was estimated lower in solution than in the gas phase (2.3–2.4% *vs*. 4%). Solvation effects on the coordination preference through the N3 atom are however limited as the Boltzmann distribution of the N3- and N2-coordinated isomers of **ZnTPP-L1** is similar in CH_2Cl_2 and DMF despite the large difference in dielectric constants.

Table 2. Calculated Zn-N distance in **ZnTPP-L1–3**, ΔH^0 for the binding of **L1–3** to **ZnTPP** and HOMO-LUMO gap.

Compound	Zn-N (Å)	ΔH^0 (kJ/mol)	HOMO-LUMO gap (eV)
B3LYP/6–31G* (Gas phase)			
ZnTPP			2.82
ZnTPP-L1			
(N2 coordination)	2.256	-42.8	2.71
(N3 coordination)	2.215	-50.9	2.69
ZnTPP-L2	2.201	-57.5	2.68
ZnTPP-L3	2.152	-63.7	2.67
B3LYP/6–31G* (CPCM model in CH_2Cl_2)			
ZnTPP			2.86
ZnTPP-L1–3			
(N2 coordination)	2.234	-30.1	2.71
(N3 coordination)	2.182	-39.6	2.68
ZnTPP-L2	2.164	-44.8	2.73
ZnTPP-L3	2.131	-51.2	2.67
B3LYP/6–31G* (CPCM model in DMF)			
ZnTPP			2.86
ZnTPP-L1–3			
(N2 coordination)	2.227	-29.4	2.70
(N3 coordination)	2.182	-38.9	2.68
ZnTPP-L2	2.161	-44.2	2.74
ZnTPP-L3	2.131	-50.8	2.67

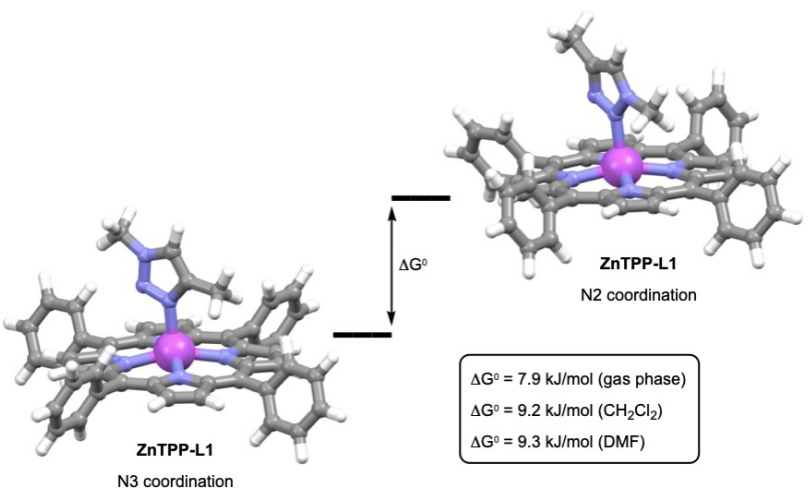

Fig. 4. DFT optimized structures and relative Gibbs free energy at 298.15 K (ΔG^0) for the two isomeric **ZnTPP-L1** complexes. Boltzmann distribution at 298.15 K for the N3-/N2-coordinated **ZnTPP-L1** complexes: 96/4 (gas phase), 97.6/2.4 (CH_2Cl_2) and 97.7/2.3 (DMF).

Analysis of the enthalpy difference (ΔH^0) for the coordination of ligand **L1** through N2 or N3 to the Zn(II) center of **ZnTPP** is also consistent for the preferential interaction of the metal with the more electronegative N atom of the triazole heterocycle. Comparison of the ΔH^0 values for the binding of **L1-3** to **ZnTPP** reflects well the affinity of the different ligands for **ZnTPP**. The strongest ligand is imidazole **L3** followed by pyridine **L2** and the weakest one is triazole **L1**. These relative affinities follow perfectly experimental trends reported for the binding of imidazole, pyridine, and 1,2,3-triazole ligands to **ZnTPP** [5, 23]. The red-shifted absorption of both the Soret and the Q bands of the porphyrin chromophore upon binding of *N*-ligands to **ZnTPP** is a diagnostic spectroscopic signature for the complexation [24]. The lower HOMO-LUMO gap found for **ZnTPP-Ln** (n = 1, 2 or 3) when compared to **ZnTPP** is thus in perfect agreement with the experimental data. The absorption spectra of **ZnTPP** and **ZnTPP-Ln** (n = 1, 2 or 3) were also calculated. Whatever the ligand, the calculated UV/vis allowed transitions were all significantly red-shifted in the complexes when compared to **ZnTPP** in good agreement with experimental observations.

The factors controlling the coordination trends of **L1-3** with **ZnTPP** were further elucidated using the interaction energy decomposition method [25]. This analysis decomposes the electronic energy of the **ZnTPP-L** complexes into two terms: the distortion energy (ΔE_{dist}) which corresponds to the energy required for the deformation of the individual components (**ZnTPP** and **L1-3**) to form the complex and the interaction energy (ΔE_{int}) which corresponds to the difference between the electronic energies of the two distorted components and the complex. The energy gain for the complexation of the *N*-ligand to the metal center of **ZnTPP** was then evaluated by adding the positive distortion energy to the negative interaction energy. The calculated energy values are summarized in Table 3.

The interaction energy and the energy gain are increased when the basicity of the ligand is increased. In the gas phase, the Zn-N distances in the DFT-optimized structures of **ZnTPP-Ln** (n = 1, 2, or 3) are shortened when the binding interaction of the *N*-ligand to the metal center is increased. This is also the case in CH_2Cl_2 and DMF. Interestingly, the Zn-N distances are however significantly affected by the solvation. They are effectively shorter when going from the gas phase to the solution. At the same time, their enthalpy differences and their interaction energies are decreased suggesting weaker binding interactions in solution. This observation is counterintuitive. However, for dative bonds, the widely accepted assumption that stronger bonds are shorter than weaker ones is not generally correct as the bond distances are very sensitive to the environment [24]. In coordination compounds, the strength of dative bonds in which the two electrons shared in the bond are provided by the ligand donor to the metal acceptor is typically destabilized by the solvent [26].

Table 3. Distortion/interaction analysis.

Compound	ΔE_{dist} [a] (kJ/mol)	ΔE_{int} [b] (kJ/mol)	$\Delta E_{dist} + \Delta E_{int}$ (kJ/mol)
B3LYP/6–311+G** (Gas phase)			
ZnTPP-L1			
(N2 coordination)	27.2	-47.1	-19.9
(N3 coordination)	29.4	-57.8	-28.4
ZnTPP-L2	26.2	-64.3	-38.1
ZnTPP-L3	31.7	-71.6	-39.9
B3LYP/6–311+G** (CPCM model in CH_2Cl_2)			
ZnTPP-L1–3			
(N2 coordination)	25.9	-30.3	-4.4
(N3 coordination)	29.7	-43.9	-14.2
ZnTPP-L2	24.5	-46.9	-22.4
ZnTPP-L3	30.6	-55.2	-24.6
B3LYP/6–311+G** (CPCM model in DMF)			
ZnTPP-L1–3			
(N2 coordination)	25.9	-29.4	-3.5
(N3 coordination)	25.9	-39.2	-13.3
ZnTPP-L2	23.9	-45.5	-21.6
ZnTPP-L3	29.0	-52.6	-23.6

[a] $\Delta E_{dist} = (E_{Frag}{}^{Zn} + E_{Frag}{}^{L}) - (E^{Zn} + E^{L})$, where $E_{Frag}{}^{Zn}$ is the electronic energy of the Zn(II)porphyrin fragment, $E_{Frag}{}^{L}$ is the electronic energy of the ligand fragment, E^{Zn} is the electronic energies of **ZnTPP** and E^{L} is the electronic energy of the ligand.

[b] $\Delta E_{int} = E - (E_{Frag}{}^{Zn} + E_{Frag}{}^{L})$, where E is the electronic energy of the complex.

Finally, we were also interested in fully rationalizing the electrochemical properties of Zn(II)porphyrins coordinated to 1,2,3-trazole ligands. As mentioned in the introduction, electrochemistry has been used to control the folding/unfolding of multi-Zn(II)-porphyrinic arrays **2** and **3**. As a typical example, the experimental observations done for compound **3** are summarized in Fig. 5.

In the neutral state, compound **3** is partially folded. The coordinated and uncoordinated Zn(II)-porphyrin moieties of **3** gave rise to different oxidation and reduction waves ($E_1{}^{ox}$ and $E_2{}^{ox}$ - $E_1{}^{Red}$ and $E_2{}^{Red}$) [12]. In both cases, the dynamic interconversion process between coordinated and uncoordinated redox centers does not occur within the voltammetric timescale. Upon complete oxidation of the ten peripheral Zn(II)-porphyrin subunits of **3**, a single wave ($E_3{}^{ox}$) has been observed for the ten peripheral radical cations suggesting that they are all coordinated in $\mathbf{3}^{10+}$. When compared to a model Zn(II) porphyrin, this third oxidation is effectively more difficult. In agreement with literature data [22, 24], this is a diagnostic signature for a coordinated Zn(II)-porphyrin radical cation. Therefore, the complete oxidation of

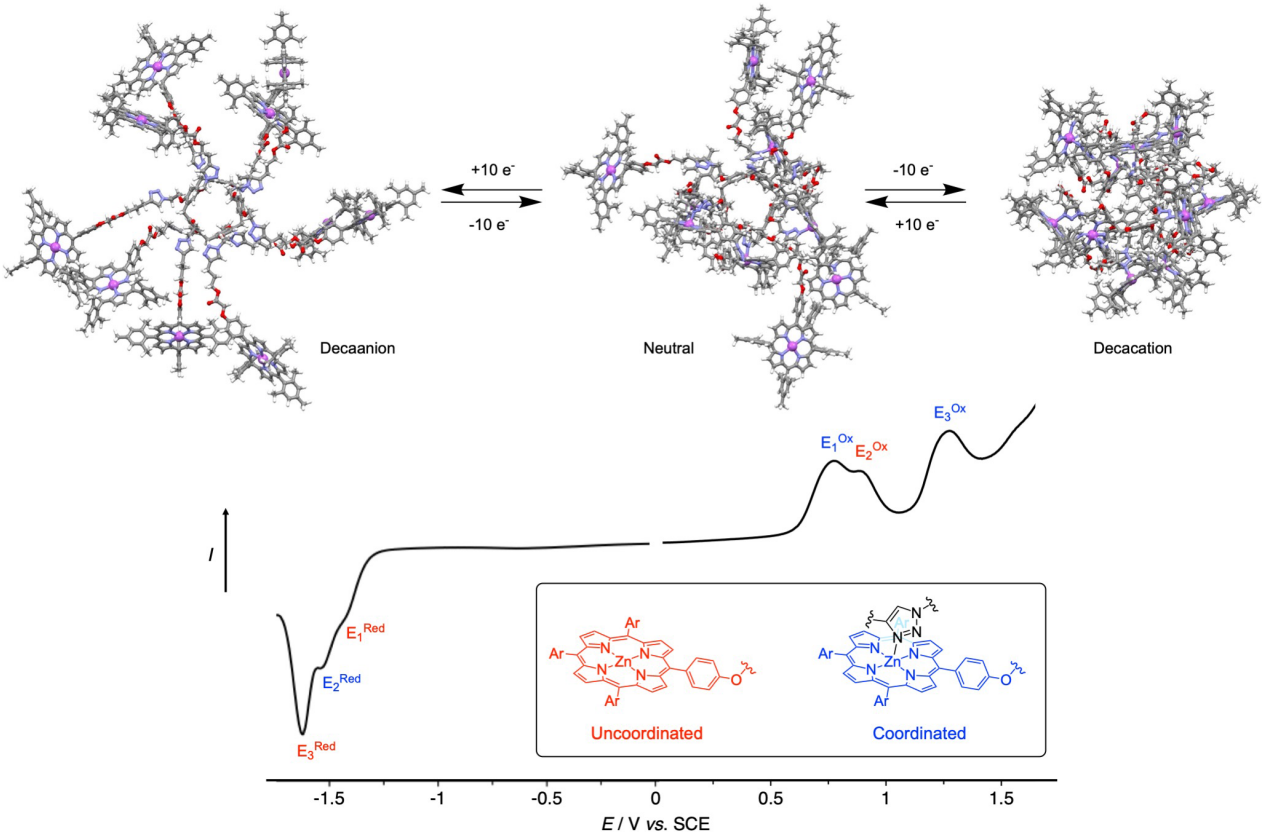

Fig. 5. Top: schematic representation of the electrochemically triggered conformational changes of compound **3**. Bottom: Osteryoung square wave voltammograms (anodic and cathodic scans) recorded for compound **3** on a Pt electrode in CH_2Cl_2 + 0.1 M nBu$_4$N.BF$_4$ at room temperature [12].

the ten peripheral Zn(II)porphyrins triggers a complete folding of the compound. In contrast, total decoordination occurs upon complete reduction of the ten peripheral Zn(II)-porphyrins thus leading to a fully unfolded deca-anion. A single wave (E_3^{Red}) is effectively observed for the reduction of the ten peripheral anionic residues at a redox potential typical for a second reduction of an uncomplexed Zn(II)-porphyrin system. All these experimental observations revealed dramatic changes in the binding ability of the 1,2,3-triazole ligand to the metal center depending on the redox state of the Zn(II)-porphyrin moiety. On the other hand, the redox properties of the Zn(II)-porphyrin unit are also modulated by the coordination of the triazole ligand. This prompted us to evaluate the binding interactions and the electronic properties of **L1** with oxidized and reduced **ZnTPP**. For this purpose, the geometries of **ZnTPP** and **ZnTPP-L1** were optimized at the B3LYP/6-31G* level for the different redox states. Both N2- and N3-coordinated isomers of **ZnTPP-L1** were analyzed. Further calculations were also performed with **L3** (see ESI). For the sake of clarity, only the most stable N3-coordinated isomer of **ZnTPP-L1** is discussed in the present section, the general trend is the same for all the systems. The calculated electron affinity (EA) and ionization potential (IP) of **ZnTPP** and N3-coordinated **ZnTPP-L1** are listed in Table 4. Relevant energetic and

Table 4. Calculated first and second electron affinities (EA_1 and AE_2), and first and second ionization potentials (IP_1 and IP_2).

Compound	EA_1 (eV)	EA_2 (eV)	IP_1 (eV)	IP_2 (eV)
ZnTPP	1.1	1.7	5.9	8.8
ZnTPP-L1	0.8	2.1	5.4	8.5

structural parameters of the complexes obtained by association of **L1** with **ZnTPP**$^{2+}$, **ZnTPP**$^{+\bullet}$, **ZnTPP**$^{-\bullet}$, and **ZnTPP**$^{2-}$ are reported in Table 5.

Table 5. Calculated Zn-N distance in the B3LYP/6–31G(d) optimized N3-coordinated **ZnTPP-L1** complexes

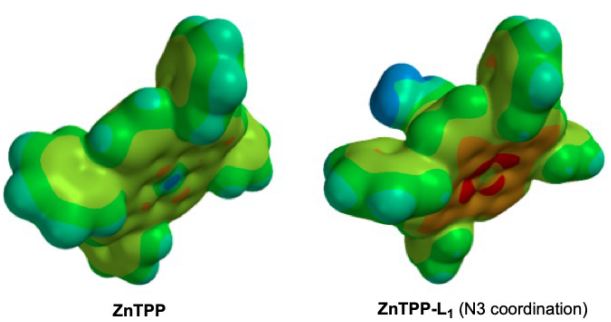

Fig. 6. Electrostatic potential map of **ZnTPP** and **ZnTPP-L1**.

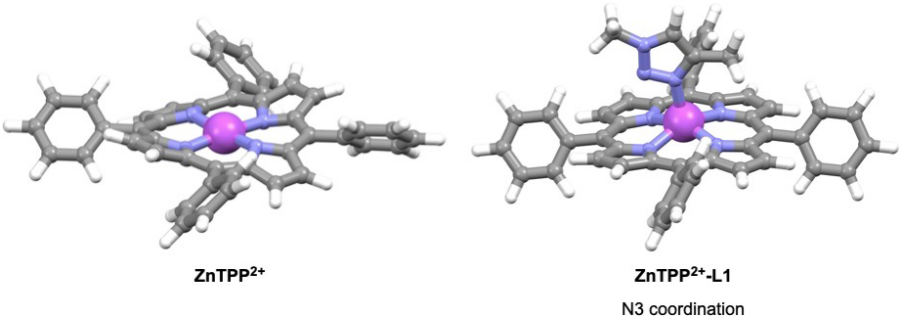

Fig. 7. DFT optimized structures of dications **ZnTPP**$^{2+}$ and **ZnTPP**$^{2+}$**-L1**.

at different redox states (gas phase), ΔH^0 for the binding of **L1** to the metal center of the Zn(II)-porphyrin, and distortion/interaction analysis from the energies calculated at the B3LYP/6–311+G** level. An ΔE_{dist} and ΔE_{int} were calculated assuming that the charge is localized on the porphyrin moiety.

When triazole ligand **L1** is interacting with **ZnTPP**, the Zn(II)-porphyrin unit is more electron-rich when compared to uncoordinated **ZnTPP**. This can be conveniently visualized by comparing the electrostatic potential map of **ZnTPP** and **ZnTPP-L1** (Fig. 6). Intuitively, the first reduction is expected more difficult in the complex. This was confirmed by the difference in the first electron affinity (EA_1) calculated for **ZnTPP** and **ZnTPP-L1**. Based on the ΔH^0 values, the complexation of **L1** to radical-anion **ZnTPP**$^{\bullet}$ is less favorable when compared to **ZnTPP**. The interaction energy is also considerably reduced and considering the distortion energy, the overall energy gain for the complexation is almost non-existent. This is in full agreement with the observed decoordination upon the first reduction of the ten peripheral Zn(II)-porphyrin moieties of compound **3**. Upon the second reduction, the enthalpy difference for the association of **L1** with **ZnTPP**$^{2-}$ is positive. The interaction energy between **ZnTPP**$^{2-}$ and **L1** is also extremely low and unable to compensate for the distortion energy. The formation of **ZnTPP**$^{2-}$**-L1** is thus thermodynamically unfavorable.

Upon oxidation of **ZnTPP**, an opposite trend is observed. The binding of **L1** to radical-cation **ZnTPP**$^{+\bullet}$ and dication **ZnTPP**$^{2+}$ is enthalpically more favorable when compared to neutral **ZnTPP**. The binding interactions of **L1** with the oxidized forms of **ZnTPP** are also considerably increased. This is fully consistent with the complete folding observed for compound **3** upon oxidation of the ten peripheral Zn(II)-porphyrin moieties. As far as the redox potential of the first oxidation is concerned, the complexation of **L1** to **ZnTPP** leads to a smaller first ionization potential (IP_1) value meaning that less energy is required to oxidize the Zn(II)-porphyrin subunit in the complex. This is fully consistent with electrochemical data and DFT calculations reported for related imidazole-Zn(II)porphyrin complexes [22] and supports the assignment for E_1^{ox} and E_2^{ox} in the voltammograms obtained for compound **3**. However, the second ionization potential (IP_2) is not in agreement with the experimental findings which revealed that the second oxidation is more difficult for complexed Zn(II)-porphyrins. The complexation of **L1** to dication **ZnTPP**$^{2+}$ is associated with a particularly large distortion energy. Indeed, the dicationic porphyrin moiety of **ZnTPP**$^{2+}$**-L1** is unable to adopt the saddle-shaped conformation observed for the uncomplexed **ZnTPP**$^{2+}$ dication because of the steric hindrance resulting from the presence of the *N*-ligand bound to the Zn(II) center (Fig. 7). Moreover, the dihedral angles between the porphyrin and the meso-phenyl substituents are significantly larger in **ZnTPP**$^{2+}$**-L1** when compared to **ZnTPP**$^{2+}$ thus reducing possible π-conjugation that may play a role in the stabilization of the dicationic Zn(II)-porphyrin moiety [22]. The positive shift observed for the second oxidation of the complexed Zn(II)porphyrin subunit must therefore result from a destabilization of the dication and not from a substantial stabilization of the intermediate radical cation.

CONCLUSION

DFT studies of the binding interactions between 1,4-disubstituted 1,2,3-triazole ligands and the metal center of Zn(II)-porphyrins revealed preferential coordination through the most electron-rich N3 atom. However, the energy difference between the N2- and N3-coordinated isomers is moderate and the less stable is likely also present in the solution. When compared to imidazole and pyridine ligands, the binding energy of 1,4-disubstituted 1,2,3-triazole derivatives to the metal center of Zn(II)-porphyrins is substantially weaker. This is related to a reduced atomic charge of the unsubstituted sp^2-hybridized N atom in the triazole heterocycle leading to a weaker basicity when compared to imidazoles and pyridines. Finally, the binding of 1,4-disubstituted 1,2,3-triazole ligands to oxidized and reduced Zn(II)-porphyrins has been also investigated. Upon reduction, the binding interactions are extremely weak and the formation of the complex is not favorable anymore. In contrast, the binding energy is considerably increased upon oxidation of the Zn(II)-porphyrin moiety thus leading to

more stable complexes. The calculations fully support the experimental observations reported for multiporphyrin arrays **2** and **3** and support the proposed conformational changes upon oxidation or reduction of their peripheral Zn(II)-porphyrin subunits. They also explain the differences in redox potentials observed for the coordinated and uncoordinated Zn(II)-porphyrin residues in compounds **2** and **3**.

Acknowledgments

Financial support by the ANR (projects FastGiant ANR-17-CE07-0012-01 and Pillar ANR-19-CE06-0032), the *Fondation Jean-Marie Lehn,* and the LabEx "Chimie des Systèmes Complexes" is gratefully acknowledged.

Supporting information

Additional data are given in the supplementary material. This material is available free of charge *via* the Internet at https://www.worldscientific.com/doi/suppl/10.1142/S1088424623500803

REFERENCES

1. (a) Kolb HC, Finn MG and Sharpless KB. *Angew. Chem. Int. Ed*. 2001; **40**: 2004–2021. (b) Tornoe CW, Christensen C and Meldal M. *J. Org. Chem*. 2002, **67**: 3057–3064. (c) Rostovtsev VV, Green LG, Fokin VV and Sharpless KB. *Angew. Chem. Int. Ed*. 2002; **41**: 2596–2599.
2. Chandrasekaran S. (Ed.), *Click Reactions in Organic Chemistry*, Wiley-VCH, Weinheim, 2016.
3. Schulze B and Schubert US, *Chem. Soc. Rev*. 2014; **43**: 2522–2571.
4. (a) Crowley JD and McMorran DA. *Top. Heterocycl. Chem*. 2012; **28**: 31–84. (b) Vasdev RAS, Preston D and Crowley JD. *Dalton Trans.* 2017; **46**: 2402–2414. (c) Elliott PI, in *Organometallic Chemistry* (Fairlamb IJS and Lynam JM, Eds), RSC, Cambridge, 2014; **39**: 1–25.
5. Nguyen NT, Mamardashvili M, Kulikova OM, Scheblykin IG, Mamardashvili NZ and Dehaen W. *RSC Adv.* 2014; **4**: 19703–19709.
6. Maeda C, Yamaguchi S, Ikeda C, Shinokubo H and Osuka A. *Org. Lett.* 2008; **10**: 549–552.
7. Maeda C, Kim P, Cho S, Park JK, Lim JM, Kin D, Vura-Weis, Wasielewski MR, Shinokubo H and Osuka A. *Chem. Eur. J*. 2010; **16**: 5052–5061.
8. Tse YC, Hein R, Mitchell EJ, Zhang Z and Beer PD. *Chem. Eur. J.* 2021; **27**: 14550–14559.
9. Mullen, KM and Gunter MJ. *J. Org. Chem*. 2008; **73**: 3336–3350.
10. (a) Wolf M, Ogawa A, Bechtold M, Vonesch M, Wytko JA, Oohora K, Campidelli S, Hayashi T, Guldi DM and Weiss J. *Chem. Sci.* 2019; **10**: 3846–3853. (b) Miyazaki Y, Kahlfuss C, Ogawa A, Matsumoto T, Wytko JA, Oohora K, Hayashi T and Weiss J. *Chem. Eur. J.* 2017; **23**: 13579–13582.
11. Kimura M, Nakano Y, Adachi N, Tatewaki Y, Shirai H and Kobayashi N. *Chem. Eur. J.* 2009; **15**: 2617–2624.
12. Trinh TMN, Nierengarten I, Ben Aziza H, Meichsner E, Holler M, Chessé M, Abidi R, Bijani C, Coppel Y, Maisonhaute E, Delavaux-Nicot B and Nierengarten JF. *Chem. Eur. J.* 2017; **23**: 11011–11021.
13. (a) Collin JP, Durola F, Heitz V, Reviriego F, Sauvage JP and Trolez Y. *Angew. Chem. Int. Ed*. 2010; **49**: 10172–10175. (b) Roberts DA, Schmidt TW, Crossley MJ and Perrier S. *Chem. Eur. J.* 2013; **19**: 12759–12770. (c) Delavaux-Nicot B, Ben Aziza H, Nierengarten I, Trinh TMN, Meichsner E, Chessé M, Holler M, Abidi R, Maisonhaute E and Nierengarten JF. *Chem. Eur. J*. 2018; **24**: 133–140.
14. (a) D'Souza F and Ito O. *Chem. Commun.* 2009: 4913–4928. (b) Nierengarten JF. *Eur. J. Inorg. Chem*. 2019: 4865–4878.
15. Deppmeier BJ, Driessen AJ, Hehre WJ, Hehre TS, Johnson JA, Ohlinger S and Klunzinger PE. *Spartan 20, Wavefunction Inc.*, Irvine CA.
16. Becke ADJ. *Chem. Phys*. 1993; **98**: 5648–5652.
17. (a) Zhang X and Herbert JM. *J. Phys. Chem. B* 2014; **118**: 7806–7817. (b) Lange AW and Herbert JM, *Chem. Phys. Lett.* 2011; **509**: 77–87. (c) Truong TN and Stefanovich EV. *Chem. Phys. Lett.* 1995; **240**: 253–260. (d) Barone V and Cossi M, *J. Phys. Chem. A* 1998; **102**: 1995–2001.
18. Tissandier MD, Cowen KA, Feng WY, Gundlach E, Cohen MH, Earhart AD, Coe JV and Tutle TR. *J. Phys. Chem. A* 1998; **102**: 7787–7794.
19. Derdel N, Clarot I, Mourer M, Regnouf-de-Vains JB and Ruis-Lopez, *J. Phys. Chem. A* 2012; **116**: 9404–9411.
20. (a) Abboub JLM, Foces-Foces C, Notorio R, Trifonov RE, Volovodenko AP, Ostrovskii VA, Alkorta I and Elguero J. *Eur. J. Org. Chem*. 2001; 3013–3024. (b) Lokov M, Tshepelevitsh S, Heering PG, Vianello R and Leito I. *Eur. J. Org. Chem*. 2017; 4475–4489.
21. (a) Zandler ME and D'Souza F. *C. R. Chimie* 2006, **9**: 960–981. (b) Tran TTH, Chang Y, Hoang, TKA, Kuo M and Su YO. *J. Phys. Chem. A* 2016; **120**: 5504–5511.
22. Tran THT, Chen GL, Hoang TKA, Kuo MY and Su YO. *J. Phys. Chem. A* 2017; **121**: 6925–6931.
23. (a) D'Souza F, Deviprasad GR, Zndler ME, Hoang VT, Klykov A, VanStipdonk M, Perera A, El-Khouly MF, Fujitsuka M and Ito O. *J. Phys. Chem. A* 2002; **106**: 3243. (b) Yoosaf K, Iehl J, Nierengarten I, Hmadeh M, Albrecht-Gary AM, Nierengarten JF and Armaroli N, *Chem. Eur. J*. 2014; **20**: 223–231.
24. Nappa M and Valentine JS, *J. Am. Chem. Soc*. 1978; **100**: 5075–5080.

25. Mo Y and Gao J. *J. Phys. Chem. A* 2001; **105**: 6530–6536.
26. (a) Lo R, Manna D, Lamanec M, Dracinsky M, Bour P, Wu T, Bastien G, Kaleta J, Miriyala VM, Spirko V, Masinova A, Nachtigollova D and Hobza P. *Nature Commun*. 2022; 13:2107. (b) Zhao L, Hermann M, Holzmann N and Frenking G. *Coord. Chem. Rev*. 2017; **344**: 163–204. (c) Zhao L, Holzmann N, Schwerdtfeger P and and Frenking G. *Chem. Rev*. 2019; **119**: 8781–8845.